Video Article

Reconstruction of 3-Dimensional Histology Volume and its Application to Study Mouse Mammary Glands

Rushin Shojaii[1], Stephanie Bacopulos[2,3], Wenyi Yang[2,3], Tigran Karavardanyan[4], Demetri Spyropoulos[5], Afshin Raouf[6], Anne Martel[1,4], Arun Seth[2,3]

[1]Department of Medical Biophysics, University of Toronto

[2]Platform Biological Sciences, Sunnybrook Research Institute

[3]Department of Laboratory Medicine and Pathobiology, University of Toronto

[4]Physical Sciences, Sunnybrook Research Institute

[5]Department of Pathology and Laboratory Medicine, Medical University of South Carolina

[6]Manitoba Institute of Cell Biology, University of Manitoba

Correspondence to: Rushin Shojaii at rushin.shojaii@sri.utoronto.ca

URL: https://www.jove.com/video/51325
DOI: doi:10.3791/51325

Keywords: Bioengineering, Issue 89, Histology Volume Reconstruction, Transgenic Mouse Model, Image Registration, Digital Histology, Image Processing, Mouse Mammary Gland

Date Published: 7/26/2014

Citation: Shojaii, R., Bacopulos, S., Yang, W., Karavardanyan, T., Spyropoulos, D., Raouf, A., Martel, A., Seth, A. Reconstruction of 3-Dimensional Histology Volume and its Application to Study Mouse Mammary Glands. *J. Vis. Exp.* (89), e51325, doi:10.3791/51325 (2014).

Abstract

Histology volume reconstruction facilitates the study of 3D shape and volume change of an organ at the level of macrostructures made up of cells. It can also be used to investigate and validate novel techniques and algorithms in volumetric medical imaging and therapies. Creating 3D high-resolution atlases of different organs[1,2,3] is another application of histology volume reconstruction. This provides a resource for investigating tissue structures and the spatial relationship between various cellular features. We present an image registration approach for histology volume reconstruction, which uses a set of optical blockface images. The reconstructed histology volume represents a reliable shape of the processed specimen with no propagated post-processing registration error. The Hematoxylin and Eosin (H&E) stained sections of two mouse mammary glands were registered to their corresponding blockface images using boundary points extracted from the edges of the specimen in histology and blockface images. The accuracy of the registration was visually evaluated. The alignment of the macrostructures of the mammary glands was also visually assessed at high resolution.

This study delineates the different steps of this image registration pipeline, ranging from excision of the mammary gland through to 3D histology volume reconstruction. While 2D histology images reveal the structural differences between pairs of sections, 3D histology volume provides the ability to visualize the differences in shape and volume of the mammary glands.

Video Link

The video component of this article can be found at https://www.jove.com/video/51325/

Introduction

IGFBP7 (insulin like growth factor binding protein 7) is a member of the IGF-binding protein family, and has been shown to bind the IGF1 receptor[4]. Down-regulation of IGFBP7 is known to be correlated with poor prognosis in breast cancer[5], while the reintroduction of IGFBP7 in Xenograft tumor models greatly inhibits the tumors growth[6] through induction of apoptosis and cellular senescence[7]. In order to study the effects of IGFPB7, an Igfbp7-null mouse was created[5] (unpublished data). While these mice do not develop tumors, they show changes in histology of the ovary, muscle and liver as well as defects in mammary gland developmental patterning (unpublished data). The defective phenotype was first indicated as the null mice have smaller litter sizes and are unable to sustain multiple large litters (unpublished data).

3D histology volumes have the potential to provide useful information for quantitative and comparative analyses and assessment of pathologic findings in volumetric medical images. Three-dimensional confocal, two-photon microscopy can provide high-resolution cell morphological information of the gland at local extent[14] , but it has a limited field of view and depth. Histology volume reconstruction provides more information over a much greater spatial extent. Using traditional approaches some distortion is anticipated during the preparation of histological sections, such as shrinkage, expansion, tears, and folds. These distortions make it difficult to register serial histological images into a 3D stack to reconstruct a 3D volume. As the number of consecutive sections with defects increases the similarities between intact sections is reduced and consequently makes the registration process more complicated.

Different methods have been proposed to register histological sections and to create a continuous histology volume. Some techniques depend on intensity variations[8], and others are based on the shape of the sections[9]. For some specimens the anatomical structures can be used as landmarks[10,11] along with landmark-based registration methods[12,13]. But these internal structures might not be detectable throughout the whole volume and for some specimens no reliable anatomical structures can be identified. Some groups have used a pair-wise registration approach

and registered consecutive histology images one to another using contours or anatomical structures[16-18]. Registering serial histology sections to one another without the use of reference images may propagate registration error and change the actual shape of the histology volume. Pair-wise registration approach relies on the consistency of shape of the histology sections and the internal structures throughout the stack of the images; therefore it requires dense sampling of the specimen, which might not always possible, *e.g.,* for clinical specimens.

In this pipeline we use blockface images as a set of reference images for histology volume reconstruction[19]. Blockface images are taken of the paraffin tissue blocks after mounting on the microtome and before each section is cut. Thus, damage to individual serial sections cut does not interfere with registration of serial sections[8,11,15]. We capture the blockface images in a different way from the other groups. The optical block face images are obtained by a telecentric lens to eliminate or minimize the barrel and perspective distortion, which usually occurs when using regular lenses in optics. This is one of the advantages of the proposed approach over the other published methods, which perform blockface imaging using regular lenses. The images are taken at a slight oblique angle to use the reflection of the surface of the block for contrast enhancement between the tissue and paraffin surface and to eliminate the shadow of the tissue in depth, under the paraffin surface. A photographic filter is also used to polarize the light coming from the block surface and the tissue to balance the contrast[19]. To correct for the displacement of the block on the rotary microtome, two to three holes are drilled in the corners of the block, which are easily detectable in the blockface images. The centroids of these holes are used along with landmark-based rigid registration to align the blockface images.

Protocol

1. Specimen

1. Excise the mammary glands surgically from wild-type CDH1 as well as Igfbp7-null mice three days post onset of lactation.
2. Spread the glands onto glass slides to help regain native mammary gland morphology.

2. Fixation and Tissue Processing

1. Fix the mammary glands in neutral buffered 4% PFA O/N at 4 ^{o}C.
2. Store the glands in 70% ethanol prior to tissue processing.
3. Transfer the glands to small tissue processing cassettes.
4. Process the tissues using an automated tissue processor
    1. Dehydrate the tissues in increasing ethanol and xylene baths of 70% ethanol for 45 min, 2 times in 95% ethanol for 45 min, 3 times in 100% ethanol for 1 hr and 2 times in xylene for 45 min.
    2. Permeate the tissues with paraffin 3 times for 1 hr each in a vacuum with applied pressure.
5. Embed the tissues in paraffin to form blocks, for sectioning.

3. Histology and Blockface Imaging

1. Trim the paraffin blocks using a rotary microtome until the excess paraffin is removed.
2. Use a vertical milling machine to drill 1 mm holes in at least two corners of the paraffin block perpendicular to the cassette.
3. Mount the tissue block on the rotary microtome.
4. Set up the blockface imaging system[19] in front of the microtome.
5. Capture optical blockface image prior to sectioning.
6. Cut ribbons of four sections at 5 µm thickness on the microtome.
    1. Transfer the ribbons to the cold water bath.
    2. Separate the second and fourth sections of the ribbon and mount them on microscope slides. Choosing the second and fourth sections provides a 5 µm gap between sections.
    3. Expand each section in a warm water bath (48 ^{o}C) to unwrinkle it, then re-mount it on the microscope slide.
    NOTE: Cutting, mounting, unwrinkling the sections cause some distortions on the section, such as tear, fold, shrinkage, and expansion. These artifacts complicate the registration of the histology sections.
    4. Stain the sections with H&E using an automatic stainer.
    5. Coverslip the slides using an automatic coverslipper.
    6. Digitize the slides using a digital histology slide scanner at the resolution of interest. For this protocol the magnification is 20x and the resolution is 0.47 µm.
    7. Down-sample the histology images to the resolution of blockface images, 18 µm.

4. Image Registration

1. Image Segmentation and point Selection
    1. In blockface images measure the pixel values of the registration holes and use the average value as a fixed threshold to segment the registration holes in the corners of the paraffin block.
    2. Since some additional parts might also be segmented by using the fixed threshold, use the circularity and the area of the segmented objects to find the holes and discard the extra objects. To do this, write a small code and find the ratio of $(4\pi \times \text{area})/(\text{perimeter})^2$ for the segmented objects. This ratio for round objects is 1.
    3. For each mammary gland, select one blockface image as reference and align the rest of the blockface images to the reference by using the centre of the registration holes and landmark-based registration techniques.

4. For the aligned blockface images, manually segment or extract the tissue from the background. Use the most sizable object in the mask for the rest of the protocol.
5. For H&E sections follow the steps below for automatic segmentation.
    1. Use Otsu thresholding technique[20] to segment images from the background and create binary masks of the histology images.
    2. Identify and select the most sizable object in each mask using the histogram of the labeled objects.
    3. Extract the one pixel wide boundary points from both histology and blockface masks.
    4. Use Chain code algorithm[21], to represent the boundary points by a sequence of piecewise linear fits.

2. Initial Rigid Registration
    1. Use Fourier Descriptors algorithm[22], to find the initial rigid transform between the boundary points of histology and their corresponding blockface images. This initial transform includes the translation, rotation and scale factors.
    2. Transform each histology image with the initial transform obtained from the previous step.

3. Refinement of the Rigid Registration
    1. Remove the high curvature edge sections from the histology contour using a rolling ball filter[23].
    2. Select 500 points from the remaining histology boundary points randomly using uniform distribution.
    3. Transform the the histology random boundary points with the initial transformation obtained from Fourier descriptors.
    4. Select the whole set of blockface boundary points and use Iterative Closest Points (ICP) algorithm[24] to find the rigid transformation between the blockface boundary points, destination, and histology random boundary points.
    5. Transform the aligned histology images obtained from the previous step and the stack of aligned histology images creates the histology volume.
    6. Use a 3D visualization software to create a visual image of the histology volume.

4. Viewing the Stack of Images at 5x magnification
    1. Down-sample the original histology images to 5x magnification.
    2. Crop the region of interest in one of the histology images.
    3. Calculate the location of that region in other 5x histology images using the combination of the rigid transformations from the two steps of registration.
    4. Crop the regions of interest to the same size region in all other histology images.
    5. Finally refine the alignment between the regions manually. Write a program that overlays two images and allows for selecting the values for rotation and translation of one of the images over the other one and then saves the transformed image when the alignment is accepted.
    6. View the stacks of the aligned 5x histology regions using a 3D visualization software.

Representative Results

A pitfall of traditional microscopy techniques is that the understanding of an organ at the microscopic level is limited to one field-of-view at a time. Even “total disclosure” slides, which provide entire slide sections, fail to provide three-dimensional information. With the development of whole slide, dynamic scanning technologies, our ability to see a section in its entirety has increased, however extrapolating structures requires 3D histology volume reconstruction.

To better characterize the deficiency of the Igfbp7-null mouse, 3D-reconstruction of mammary glands were performed on glands excised 3 days post commencement of lactation. **Figure 1** shows the pipeline of the proposed approach for 3D histology reconstruction. The blockface images are first aligned using the holes in the corners of the paraffin block. **Figures 2A-B** show the blockface volume of the wild-type and Igfbp7-null mammary glands respectively. The histology images are then registered to their corresponding aligned blockface images to reconstruct the histology volumes. **Figures 3A-B** show the reconstructed histology volumes of the wild-type and Igfbp7-null mammary glands. By looking at the overall structures (videos A and B) we can see the difference in size between mutant and wild type glands. However, using the approach described herein, it becomes apparent that this size difference is in length and width but interestingly not depth. For the glands used in this pilot experiment, the wild-type gland was 1.06 mm deep, while the Igfbp7-null gland was 1.02 mm deep. The other phenotype immediately noticeable is the difference in stromal components of the two glands, as marked by eosin staining (pink areas). The wild-type glands have little stromal tissue, while the null-glands appear to be predominantly stromal tissue. This difference is especially evident when viewing videos C and D. The videos contain only nucleated cells (staining with hematoxylin), from these videos we can see that the null gland maintains its density, while the wild-type gland appears to contain primarily glandular structures. The spacing between the sections in videos A to D has been increased to twice the original spacing to assist with the visualization. To further investigate this, images were aligned near the lymph node in higher resolution, this allows us to see how the glands are changing in serial sections. In the wild-type gland we can see large structures, which would have been filled with milk (videos E and F). In contrast the Igfbp7-null gland has few well-developed structures. Moreover, these structures were crowded with fibroblast-like cells.

As a major defect with the Igfbp7-null mouse is the ability to sustain large litters, it is evident through the comparison presented that the structural difference between the wild-type and null glands could contribute to the observed phenotype[25]. The alveolar volume is greatly reduced within the null-glands indicating inadequate milk volume for feeding large litters. We determined that the total volume of the wild-type gland was 82.8879 mm^3 while the null gland measured only 19.6291 mm^3.

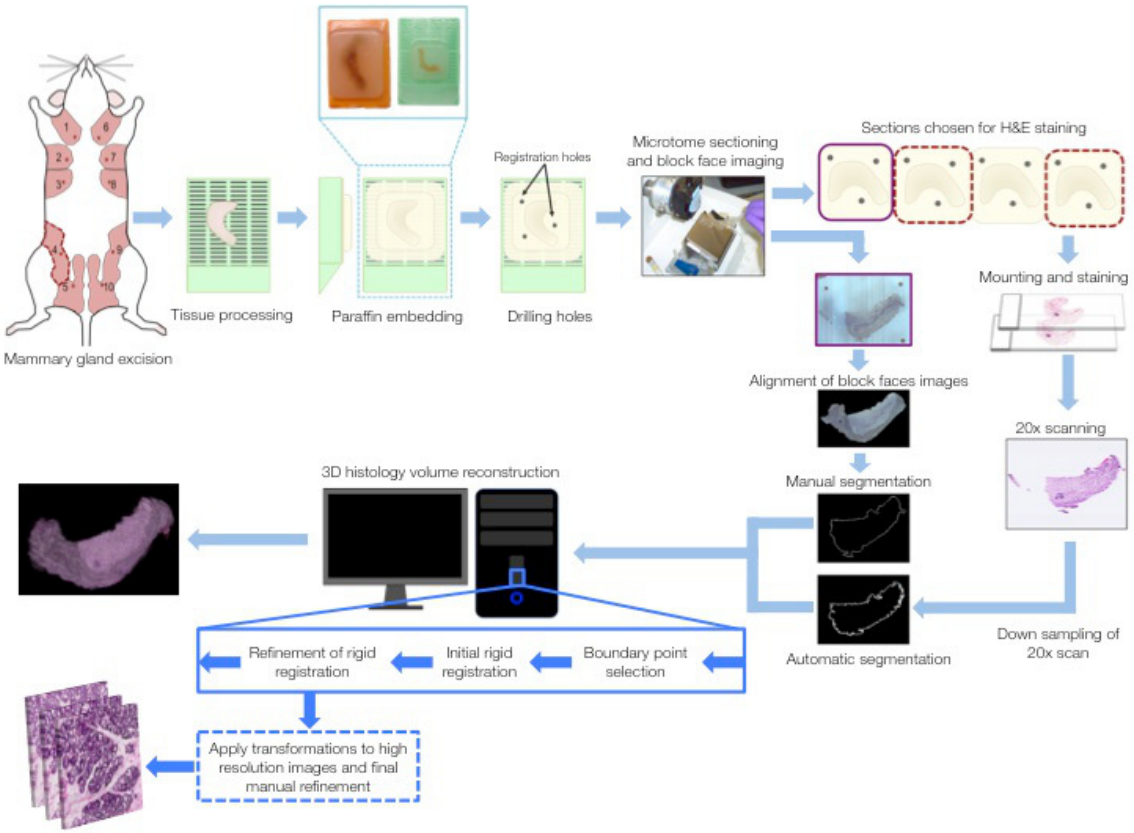

Figure 1. Schematic depicting the steps involved in the 3D reconstruction process. Fourth inguinal mouse mammary glands were used as the examples. Mammary glands were harvested from normal and null mice, then processed and paraffin embedded. Registration holes were drilled into the paraffin blocks followed by block face imaging and serial sectioning of the glands. Sections were retrieved in ribbons of four sections. The first section was block-faced imaged prior to sectioning (purple outline), while the 2nd and 4th sections (red outline) were chosen for H&E staining and scanning. Block face images were aligned (using registration holes) and manually segmented. H&E sections were digitized at 20x resolution then down-sampled; these images were automatically segmented. Both sets of segmented images were subjected to boundary point selection and registration. Outputs are 3D histological volumes as well as high-resolution areas. Please click here to view a larger version of this figure.

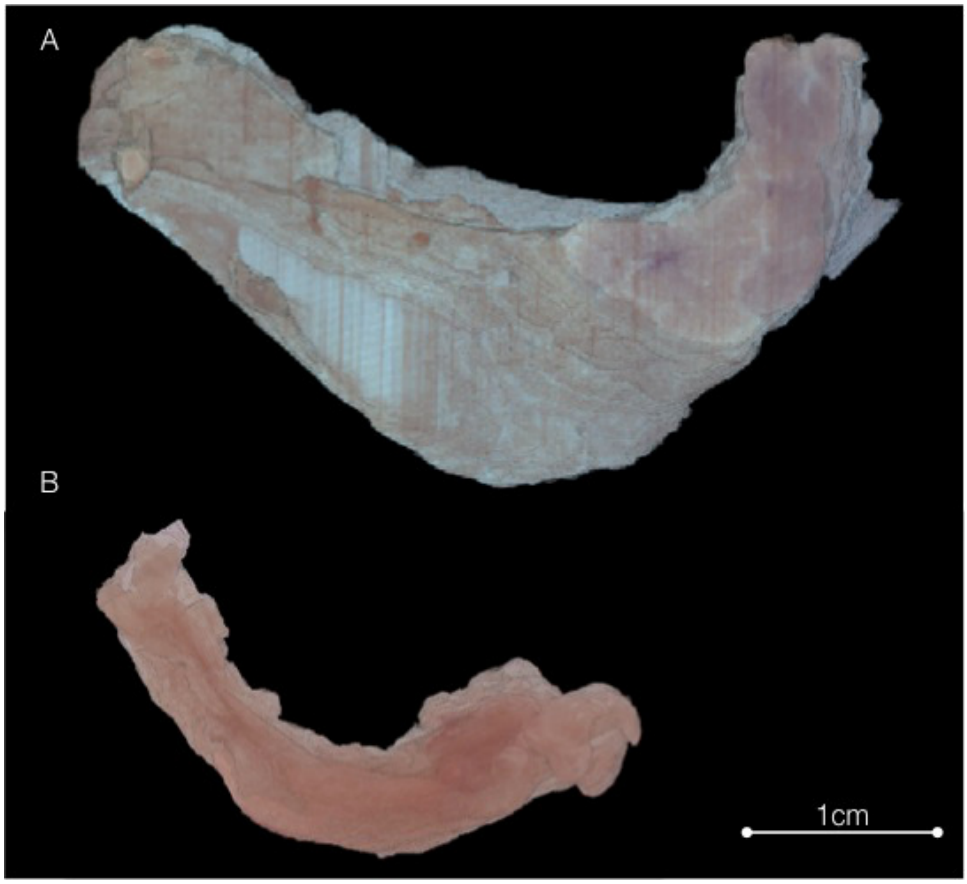

Figure 2. Blockface Volume. Optical images of the paraffin block mounted on the microtome are obtained before each section is cut. The centroid of the drilled holes at the corners of the paraffin block is used to align the blockface images and create the blockface volume. Image **(A)** shows the wild-type mammary gland at 3 days post induction of lactation and **(B)** shows the same time-point for the Igfbp7-null mammary gland. Please click here to view a larger version of this figure.

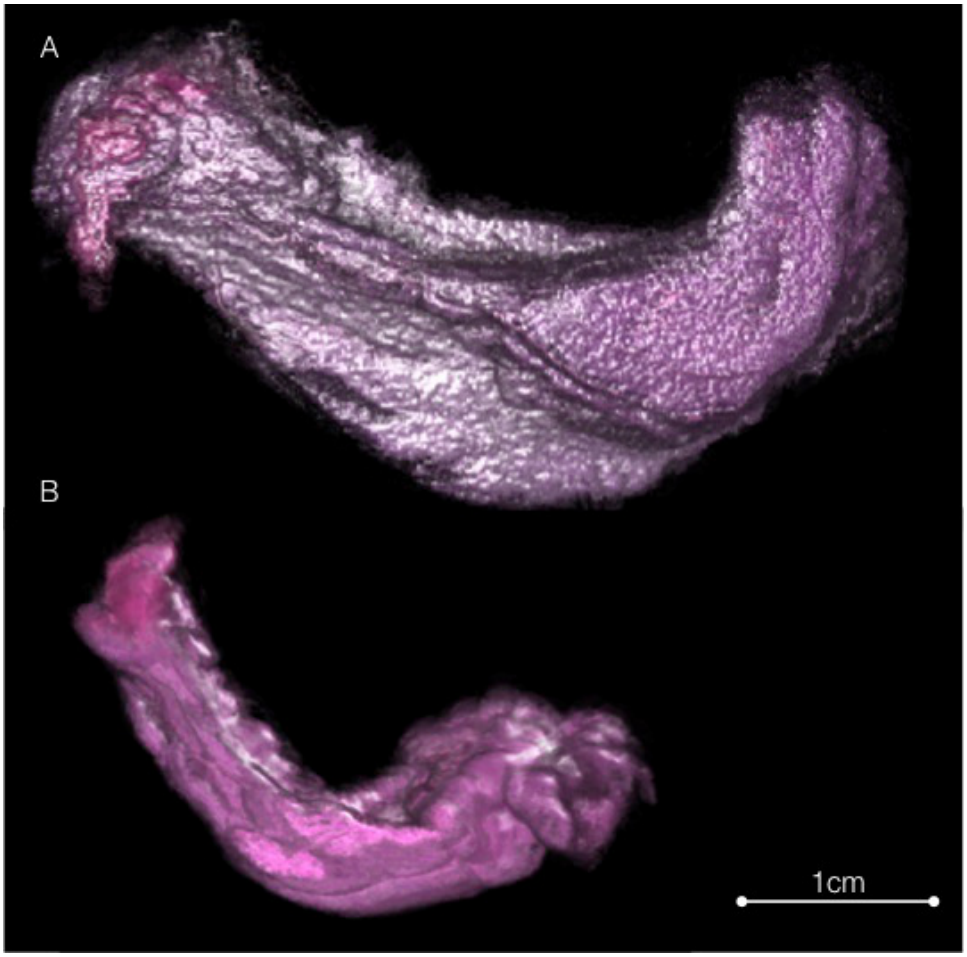

Figure 3. Histology volume. The histology images registered to their corresponding aligned blockface images to reconstruct histology volume. **(A)** Wild-type gland and **(B)** Igfbp7-null mammary gland, 3 days post lactation induction. Please click here to view a larger version of this figure.

Discussion

In this study, we have developed an image registration workflow to reconstruct a 3D histology volume from serial 2D histology images, which does not require internal randomly selected landmarks or implanted fiducial markers within the tissue, which might distort the tissue. By the method described, optical blockface images themselves are used as the reference images prior to sectioning. We use external holes drilled in the paraffin block to aid in aligning the blockface images and to correct for the 2D transversal movement of the paraffin block in front of the camera. The 2D histology images are aligned to the corresponding 2D blockface images to prevent the propagation of the registration error and reconstruct an accurate histology volume, even when defective serial sections result from blocks. In order to make the workflow independent of the type of the tissue and the histology stain used, boundary points are used to carry out the registration. This point-based approach has the advantage (over intensity-based approaches) that it is less computationally demanding and therefore better able to cope with very large digital pathology images.

Another advantage of using blockface images to align the histology images is that the spacing between the histology images does not affect the quality of their alignment to create the histology volume. This is important in the clinical setting where the spacing between sections can vary widely, often as great as half a centimeter.

Throughout this paper we have shown that the approach is reproducible for two different mammary glands with different structures and intensity variations. Since the approach uses the boundary of the sections, the degree of variation between different glands is small. Previously we have also shown the capability of the approach for another pre-clinical model[19]. As different tissue types have different biomechanical properties, the registration error is expected to change for different specimens. We think that the pipeline is applicable to fairly solid specimens, *e.g.,* human tumor xenografts. In the future we will further investigate the accuracy of the 3D reconstruction pipeline using other specimens, such as human breast tissue.

One of the other limiting factors of the proposed workflow is the manual segmentation of the blockface images. This limitation could be removed by developing an automatic texture segmentation approach, for example by using Markov Random Field (MRF) models[26,27] to segment the specimen from the background in blockface images.

Through the examination of the wild-type and Igfbp7-null mammary glands, we were able to identify differences in the structure and composition of the glands in 3D through a comprehensive composite of the individual sections of both glands. This technique aided in further characterizing

the Igfbp7-null phenotype at the cellular level, and showed that distinct differences in alveolar volume may contribute to some of the defects seen in this model[25].

The important capability of this approach is that it is independent from the tissue type and intensity variations and thus it can be used to reconstruct the histology volume of different pre-clinical and clinical specimens. One of the other advantages of this approach is that it is not dependant on a specific stain. This contour based approach is compatible with any stain, so long as it provides a clear contour of the whole section or a clear contour of a structure, which is detectable in both histology and blockface images. The investigation of the tumor shape, volume, and heterogeneity is one of the clinical applications of the 3D histology volume. In this paper we have shown that the proposed approach is capable of reconstruction of 3D histology volume and can be further used for comparison, visualization and analysis of other specimens.

Disclosures

The authors have nothing to disclose

Acknowledgements

The authors would like to thank the Biomarker Imaging Research Laboratory (BIRL) at Sunnybrook Research Institute for their histology services. Support for this work was provided by the Terry Fox Foundation, the Canadian Breast Cancer Foundation#the Prairie#NWT as well as a CIHR grant, #MOP-97996.

References

1. Sunkin, S.M., *et al.* Allen Brain Atlas: An integrated spatiotemporal port for exploring the central nervous system. *Nucleic Acids Research.* **41**, 996-1008, doi:10.1093/nar/gks1042 (2012).
2. Shen, E.H., Overly, C.C., & Jones, A.R. The Allen Human Brain Atlas: Comprehensive gene expression mapping of the human brain. *Trends in Neurosciences.* **35** (12), 711-714, doi:10.1016/j.tins.2012.09.005 (2012).
3. Trifunović, D., Karali, M., Camposampiero, D., Ponzin, D., Banfi, S., & Marigo V. A high-resolution RNA expression atlas of retinitis pigmentosa genes in human and mouse retinas. *Invest. Ophthalmol. Vis. Sci.* **49** (6), 2330-2336, doi:10.1167/iovs.07-1513 (2008).
4. Evdokimova, V., *et al.* IGFBP7 binds to the IGF-1 receptor and blocks its activation by insulin-like growth factors. *Science Signaling.* **5** (255), 92, doi:10.1126/scisignal.2003184 (2012).
5. Burger, A., Leyland-Jones, B., Banerjee, K., Spyropoulos, D., & Seth, A. Essential roles for IGFBP-3 and IGFBP-rP1 in breast cancer. *European J. Cancer.* **41** (11), 1515-1527, (2005).
6. Amemiya, Y., *et al.* Insulin like growth factor binding protein-7 reduces growth of human breast cancer cells and xenografted tumors. *Breast Cancer Res Treat.* **126** (2), 373-384, (2011).
7. Benatar, T., *et al*. IGFBP7 reduces breast tumor growth by induction of senescence and apoptosis pathways. *Breast Cancer Res Treat.* **133** (2), 563-573, doi:10.1007/s10549-011-1816-4 (2012).
8. Bardinet, E., *et al*. Co-registration of histological, optical and MR data of the human brain. *Medical Image Computing and Computer-Assisted Intervention-Part I.* 548-555. Springer-Verlag, London, UK, (2002).
9. Jacobs, M.A., Windham, J.P., Soltanian-Zadeh, H., Peck, D.J, & Knight, R.A. Registration and warping of magnetic resonance images to histological sections. *Medical Physics.* **26** (8), 1568-1578, (1999).
10. Zhan, Y., Ou, Y., Feldman, M., Tomaszeweski, J., Davatzikos, C., & Shen, D. Registering histologic and MR images of prostate for image-based cancer detection. *Academic radiology.* **14** (11), 1367-1381, (2007).
11. Dauguet, J., *et al.* Three-dimensional reconstruction of stained histological slices and 3D non-linear registration with *in vivo* MRI for whole baboon brain. *Journal of Neuroscience Methods.* **164** (1), 191-204, (2007).
12. Lazebnik, R.S., Lancaster, T.L., Breen, M.S., Lewin, J.S., & Wilson, D.L. Volume registration using needle paths and point landmarks for evaluation of interventional MRI treatments. *IEEE Transactions on Medical Imaging.* **22** (5), 653-660, (2003).
13. Breen, M. S., Lazebnik, R. S., & Wilson, D. L. Three-dimensional registration of magnetic resonance image data to histological sections with model-based evaluation. *Annals of Biomedical Engineering.* **33** (8), 1100-1112, (2005).
14. Mori, H., Borowsky, A.D., Bhat, R., Ghajar, C.M., Seiki, M., & Bissell, M.J. *The American Journal of Pathology.* **180** (6), 2249-2256, doi:10.1016/j.ajpath.2012.02.032 (2012).
15. Gibb, M., *et al.* Resolving the three-dimensional histology of the heart. *Computational Methods in Systems Biology.* Edited by Gilbert, D., & Heiner, M. 2-16. Springer-Verlag, London, UK, (2012).
16. Wu, M.L., *et al.* Three-dimensional virtual microscopy of colorectal biopsies. *Archives of Pathology & Laboratory Medicine.* **129** (4), 507-510, (2005).
17. Arganda-Carreras, I., *et al.* 3D Reconstruction of histological sections: Application to mammary gland tissue. *Microscopy Research and Technique.* **73** (11), 1019–1029, doi:10.1002/jemt.20829 (2010).
18. Song, Y., Treanor, D., Bulpitt, A.J., & Magee, D.R. 3D reconstruction of multiple stained histology images. *Journal of Pathology Informatics.* **4** (2), 7, doi:10.4103/2153-3539.109864 (2013).
19. Shojaii, R., Karavardanyan, T., Yaffe, M., & Martel, A.L. Validation of histology image registration. *SPIE Medical Imaging.* **7962**, 79621E, doi:10.1117/12.878762 (2011).
20. Ridler, T.W., & Calvard, S. Picture thresholding using an iterative selection method. *IEEE Transactions on Systems, Man, and Cybernetics.* **8** (8), 630-632, (1978).
21. Freeman, H. Computer processing of line-drawing images. *ACM Computing Surveys (CSUR).* **6** (1), 57–97, (1974).
22. Giardina, C. Accuracy of curve approximation by harmonically related vectors with elliptical loci. *Computer Graphics and Image Processing.* **6** (3), 277–285, (1977).

23. Shojaii, R., Martel, A.L. A novel edge point selection method for registration of histology images. *Optical Tissue Image analysis in Microscopy, Histopathology and Endoscopy.* (OPTIMHisE) Workshop, MICCAI, (2009).
24. Besl, P., & McKay, N. A method for registration of 3-D shapes. *IEEE Transactions on Pattern Analysis and Machine Intelligence.* **14** (2), 239–256, (1992).
25. Chatterjee, S., *et al.* Loss of *Igfbp7* causes precocious involution in lactating mouse mammary gland. *PLoS ONE.* **9** (2), e87858, (2013).
26. Manjunath, B.S., & Chellappa, R. Unsupervised texture segmentation using Markov random field models. *IEEE Transactions on Pattern Analysis and Machine Intelligence.* **13** (5), 478–482, (1991).
27. Krishnamachari, S., & Chellappa, R. Multiresolution Gauss-Markov random field models for texture segmentation. *IEEE Transactions on Image Processing: a publication of the IEEE Signal Processing Society.* **6** (2), 251–267, (1997).

